2016 International Symposium on Nonlinear Theory and Its Applications,
NOLTA2016, Yugawara, Japan, November 27th-30th, 2016

Chaos near the Chenciner bubbles from a piecewise-constant system

Tri Quoc TRUONG[a], Tadashi TSUBONE[a], Naohiko INABA[b] and Tetsuro ENDO[c]

[a] Department of Integrated Bioscience and Technology, Nagaoka University of Technology
1603-1 Kamitomioka, Nagaoka, Niigata 940-2188, Japan
[b] Organization for the Strategic Coordination of Research and Intellectual Properties, Meiji University
Kawasaki, Kanagawa 214-8571, Japan
[c] Department of Electronics and Bioinformatics, School of Science and Technology, Meiji University
Kawasaki, Kanagawa 214-8571, Japan
Email: qttruong@stn.nagaokaut.ac.jp, tsubone@vos.nagaokaut.ac.jp, naohiko@yomogi.jp, endoh@isc.meiji.ac.jp

Abstract—We consider chaos and bifurcation phenomena near the Chenciner bubbles generated by two coupled piecewise-constant oscillators (PWCOs) driven by a rectangular wave force. Because vector fields of PWCOs are piecewise-constants, it is relatively easy to perform rigorous analysis. For instance, a calculation algorithm for conducting Lyapunov exponent in autonomous piecewise-constant system has been proposed. By using extension of the algorithm for non-autonomous system, two-parameter Lyapunov diagrams are conducted. These results confirmed that Chaos is observed in the neighborhood of Chenciner bubbles. Furthermore, we observed the Farey sequence in the experimental measurements.

1. Introduction

Quasi-periodic bifurcations of high-dimensional tori have attracted intensive research interest in recent years. For instance, to observe bifurcation structures in discrete-time dynamics, Sekikawa et al. analyzed a coupled delayed logistic map that generated complicated quasi-periodic bifurcations [1]. Infinitely many of 2-torus generating regions existed in a 3-torus generating region, wherein 2-torus generating regions extend in numerous directions like a "cobweb" in parameter space called Arnold resonance web. The generation pattern of 2-torus regions is explained by the Farey sequence [2]. In addition, periodic solutions emerge at the intersections of two different 2-torus, which called Chenciner bubbles. The study of Arnold resonance webs is usually performed by Lyapunov analysis, and has been rapidly progressings. However, the main concerns for observing Arnold resonance webs in continuous-time dynamics are the precision and computational cost. To analyze bifurcation structures in continuous-time dynamics more precisely, Tsubone et al. proposed and analyzed piecewise-constant oscillator (PWCOs) [3]. Because vector fields of PWCOs take only constant values piecewisely, it is relatively easy to perform rigorous analysis. Hence, using the same computational cost similar to that of discrete-time dynamics, Inaba et al. succeed in observing Arnold resonance webs with high resolution in a driven continuous-time electric circuit of which governing equation is represented by two coupled piecewise-constant oscillators (PWCOs) driven by a rectangular wave force [4]. However, they obtained the Lyapunov exponents by using an ad-hoc manner. It could be difficult to apply this procedure in higher dimensional piecewise-constant dynamics. In this study, we focus on chaos and bifurcation phenomena near the Chenciner bubbles generated in a driven continuous-time electric circuit presented in [4]. The analysis is performed by using a calculation algorithm for the rigorous solutions in non-autonomous piecewise-constant system, which extended the algorithm in autonomous piecewise-constant system [5]. By using this algorithm, two-parameter Lyapunov diagrams are easily conducted. According to the numerical experiment, Chaos is observed in the neighborhood of Chenciner bubbles. Moreover, the Farey sequence is verified by laboratory measurements.

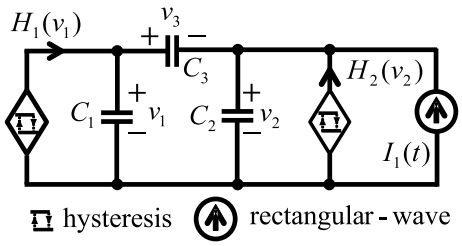

Figure 1: Piecewise-constant oscillator

2. Piecewise-constant oscillator

In this study, we consider the piecewise-constant circuit in Fig. 1. This circuit comprises two piecewise-constant hysteresis ocillators and a rectangular wave current source. The voltage across two capacitors C_1 and C_2 is v_1, v_2, respectively. $H_1(v_1)$ and $H_2(v_2)$ are the two hysteresis elements. The waveform of the rectangular wave source with amplitude I and period $2T_0$

is shown in Fig. 2. From Kirchhoff's law, the governing equation is represented as follows.

$$\begin{aligned}\frac{C_1C_2+C_1C_3+C_2C_3}{C_3}\frac{\mathrm{d}v_1}{\mathrm{dt}}&\\ =\frac{C_2+C_3}{C_3}H_1(v_1)+H_2(v_2)+I_1(t),&\\ \frac{C_1C_2+C_1C_3+C_2C_3}{C_3}\frac{\mathrm{d}v_2}{\mathrm{dt}}&\\ =\frac{C_1+C_3}{C_3}\Big(H_2(v_2)+I_1(t)\Big)+H_1(v_1).&\end{aligned} \tag{1}$$

Via rescaling,

$$\begin{gathered}v_1=V_{th1}x,\ v_2=V_{th2}y,\ t=\gamma\tau,\\ h_1(x)I_{h1}=H_1(V_{th1}x),\ h_2(y)I_{h2}=H_2(V_{th2}y),\\ \frac{\gamma I_{h1}C_3}{V_{th1}(C_1C_2+C_1C_3+C_2C_3)}=1,\\ \frac{I_{h2}}{I_{h1}}=D_1,\ \frac{V_{th1}}{V_{th2}}=D_2,\ \frac{I}{I_{h1}}=B,\\ \frac{C_2+C_3}{C_3}=D_3,\ \frac{C_1+C_3}{C_3}=D_4,\ \frac{T_0}{\gamma}=T,\end{gathered} \tag{2}$$

the normalized equation is:

$$\begin{aligned}\dot{x}&=D_3h_1(x)+D_1h_2(y)+S(\tau),\\ \dot{y}&=D_2h_1(x)+D_2D_4\big(D_1h_2(y)+S(\tau)\big).\end{aligned} \tag{3}$$

where $h_1(x)$ and $h_2(y)$ are the normalized hysteresis loops, of which characteristics are shown in Fig. 3(a) and Fig. 3(b), respectively. The solution on the upper branch ($h_1(x)=1$) jumps to the lower branch ($h_1(x)=-1$) when x increases and reaches the point S_1. In addition, the solution on the lower branch ($h_1(x)=-1$) jumps to the upper branch ($h_1(x)=1$) when x decreases and reaches the point S_2. The solution on the branch $h_2(y)$ behaves in the same manner. Periodic external force $S(\tau)$ is expressed as follow.

$$S(\tau)=\begin{cases}B\ \text{for}\ nT\le\tau<(n+1)T,\\ -B\ \text{for}\ (n+1)T\le\tau<(n+2)T.\end{cases} \tag{4}$$

where n is integer. B and T is the amplitude and half-periodic of the rectangular wave, respectively. The circuit dynamics include six parameters D_1, D_2, D_3, D_4, B, and T. Note that because of the characteris of $h_1(x)$ and $h_2(y)$, throughout this study, we restrict our attention to the case when $-1\le x(\tau)\le 1$ and $-1\le y(\tau)\le 1$ hold for $\forall\tau$. In our assumption, the trajector in vector fileds will hit boundary lines, i.e, $x=1, x=-1, y=1$, or $y=-1$.

3. Derivation of Lyapunov exponents in a driven piecewise-constant oscillator

In this section, we explain the procedure for deriving the Lyapunov exponents by introducing the explicit expression of the solution. In our previous work, the basic algorithm to calculate Lyapunov exponents

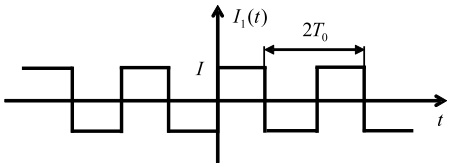

Figure 2: Rectangular wave

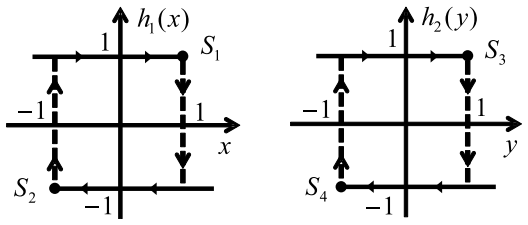

(a) (b)

Figure 3: Hysteresis loops: (a) $h_1(x)$ and (b) $h_2(y)$.

in autonomous piecewise-constant system is proposed [5]. However, the algorithm is not suitable for the non-autonomous systems, because it can not manage enforced switching depending on external force. To make it easy to conduct rigorous solutions in non-autonomous system, we assume τ in Eq. (3) as a variable. Hence, we can rewrited Eq. (3) in the autonomous form as follows.

$$\begin{aligned}\dot{x}&=k_x=D_3h(x)+D_1h(y)+S(z)\\ \dot{y}&=k_y=D_2h(x)+D_2D_4\big(D_1h(y)+S(z)\big)\\ \dot{z}&=1.\end{aligned} \tag{5}$$

We consider the solution where the initial condition at z_0 is $\boldsymbol{x_0}=(x_0,\ y_0,\ z_0)^\top$. When the trajectory started at z_0 hits a boundary line, i.e., either one of $x=1, x=-1, y=1, y=-1, z=T$, or $z=2T$ at the time z_1, the solution of Eq. (5) is expressed as follows.

$$\boldsymbol{x}_1=\boldsymbol{x}_0+\boldsymbol{k}(z_1-z_0), \tag{6}$$

where $\boldsymbol{k}=(k_x,k_y,1)^\top$ is vector fields presented by Table 1. To conduct the Jacobian matrix in a systematic manner, a normal vector $\boldsymbol{n}^\top$ is introduced. By using this normal vector, the (z_1-z_0) in Eq. (6) is obtained

$$z_1-z_0=\frac{\boldsymbol{n}^\top\boldsymbol{x}_1-\boldsymbol{n}^\top\boldsymbol{x}_0}{\boldsymbol{n}^\top\boldsymbol{k}} \tag{7}$$

Note that, at the time z_1 the trajectory is on boundary line. Thus, $\boldsymbol{n}^\top\boldsymbol{x}_1=D$ is a constant value presented in Table 2. For example, when the solution hits $x=1$, because the normal vector is $\boldsymbol{n}=(1\ 0\ 0)^\top$, the scalar D is $D=1$. In addition, substituting Eq. (7) into Eq. (6) yields the following equation.

$$\boldsymbol{x}_1=\left(I-\frac{\boldsymbol{k}\boldsymbol{n}^\top}{\boldsymbol{n}^\top\boldsymbol{k}}\right)\boldsymbol{x}_0+\frac{\boldsymbol{k}D}{\boldsymbol{n}^\top\boldsymbol{k}}. \tag{8}$$

Table 1: Values of $\boldsymbol{k}$

$\boldsymbol{k}$	Regions
$\big(D_3+D_1+B, D_2+D_2D_4(D_1+B), 1\big)^\top$	$h_1(x)=1,\ h_2(y)=1,\ 0\le z<T$
$\big(-D_3+D_1+B, -D_2+D_2D_4(D_1+B), 1\big)^\top$	$h_1(x)=-1,\ h_2(y)=1,\ 0\le z<T$
$\big(D_3-D_1+B, D_2+D_2D_4(-D_1+B), 1\big)^\top$	$h_1(x)=1,\ h_2(y)=-1,\ 0\le z<T$
$\big(-D_3-D_1+B, -D_2+D_2D_4(-D_1+B), 1\big)^\top$	$h_1(x)=-1,\ h_2(y)=-1,\ 0\le z<T$
$\big(D_3+D_1-B, D_2+D_2D_4(D_1-B), 1\big)^\top$	$h_1(x)=1,\ h_2(y)=1,\ T\le z<2T$
$\big(-D_3+D_1-B, -D_2+D_2D_4(D_1-B), 1\big)^\top$	$h_1(x)=-1,\ h_2(y)=1,\ T\le z<2T$
$\big(D_3-D_1-B, D_2+D_2D_4(-D_1-B), 1\big)^\top$	$h_1(x)=1,\ h_2(y)=-1,\ T\le z<2T$
$\big(-D_3-D_1-B, -D_2+D_2D_4(-D_1-B), 1\big)^\top$	$h_1(x)=-1,\ h_2(y)=-1,\ T\le z<2T$

It is clear from Eq. (8) that the local Jacobian matrix A is represented by

$$A=\frac{\mathrm{d}\boldsymbol{x}_1}{\mathrm{d}\boldsymbol{x}_0}=I-\frac{\boldsymbol{k}\boldsymbol{n}^\top}{\boldsymbol{n}^\top\boldsymbol{k}}. \tag{9}$$

Then, if the solution hits $x=1$ or $x=-1$,

$$A_0=\begin{pmatrix}0 & 0 & 0\\ -k_y/k_x & 1 & 0\\ -1/k_x & 0 & 1\end{pmatrix}, \tag{10}$$

if the solution hits $y=1$ or $y=-1$,

$$A_1=\begin{pmatrix}1 & -k_x/k_y & 0\\ 0 & 0 & 0\\ 0 & -1/k_y & 1\end{pmatrix}, \tag{11}$$

and, if the solution hits $z=T$ or $z=2T$,

$$A_2=\begin{pmatrix}1 & 0 & -k_x\\ 0 & 1 & -k_y\\ 0 & 0 & 0\end{pmatrix}. \tag{12}$$

Note that the Jacobian matrices A_0, A_1, and A_2 includes an all zero row. Therefore, one of eigenvalues of these matrices is zero and the corresponding minumum Lyapunov exponent is $-\infty$. Hence, we define the first and the second Lyapunov exponent as follows.

$$\begin{aligned}\lambda_1 &\simeq \frac{1}{N}\sum_{j=M+1}^{M+N}\ln\left|A_i^j e_1^j\right|\\ \lambda_1+\lambda_2 &\simeq \frac{1}{N}\sum_{j=M+1}^{M+N}\ln\left|A_i^j e_1^j\times A_i^j e_2^j\right|,\end{aligned} \tag{13}$$

where e_1^j and e_2^j are orthonomal bases. $A_i^j(=\dfrac{\mathrm{d}\boldsymbol{x}_j}{\mathrm{d}\boldsymbol{x}_{j-1}})$ is the Jacobian matrix, which is one of A_0, A_1, and A_2. M and N are integers. We use a sufficiently large N after removing the transient state. Because the precision and speed of calculation of piecewise-constant oscillator is excellent, it is desirable to choose M as large as N. It is reasonable to argue that for $M=N=2\times10^7$the two Lyapunov exponents converge to zero. Therefore, we consider as $\lambda_i=0$ if the calculated λ_i satisfies $|\lambda_i|<1/10^6$.

Table 2: Values of D

	$\boldsymbol{n}^\top$	D
$x=1$	(1 0 0)	1
$x=-1$	(1 0 0)	-1
$y=1$	(0 1 0)	1
$y=-1$	(0 1 0)	-1
$z=T$	(0 0 1)	T
$z=2T$	(0 0 1)	$2T$

4. Chenciner bubbles and Chaos generated in a piecewise-constant circuit

In this section, we fix the coupling parameters $C_3/C_1=C_3/C_2=0.01$ that correspond to $D_3=D_4=101$. We choose D_1 and T as variables and set the parameters $D_2=1.1$ and $B=0.005$. Fig. 4 shows two-parameter Lyapunov diagram. In this figure, a region generating a periodic solution marked in red where the oscillation frequencies of the two hysteresis oscillators and the forcing term are synchronized. This region can be denoted as the Chenciner bubbles. Regions generating two-dimensional tori ($\lambda_1=0, \lambda_2<0$) and three-dimensional tori ($\lambda_1=0, \lambda_2=0$) are maked in blue and yellow, respectively. Regions generating chaos are marked in black. As seen in Fig. 4 (a), the Arnold resonance web is clearly observed. Moreover, chaos is inevitably observed near the periodic solution generating region around which the regions generating three-dimensional tori emanate. Our numerical result shows against the remark given by Baesens et al. [6] that if the coupling parameter of dynamics equation is small, chaos generations cannot be observed.

To observing Farey sequence in the circuit, we set $C_3/C_1=C_3/C_2=1/10$, i.e., $D_3=D_4=11$. The nu-

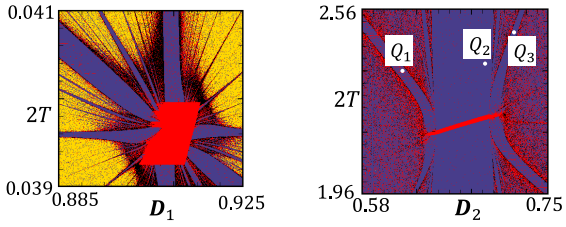

(a) (b)

Figure 4: Lyapunov diagram: (a) $D_2 = 1.1$, $D_3 = D_4 = 101$, $B = 0.005$; (b) $D_1 = 0.5$, $D_3 = D_4 = 11$, $B = 0.005$.

merically obtained two-parameter diagram is shown in Fig. 4 (b). In this case, the regions generating two-dimensional tori are relatively thin. Fig. 5 (a.1), (a.2), (a.3) show the two-dimensional tori on the section Π which are obtained at the parameter values denoted by Q_1, Q_2 and Q_3 in Fig. 4 (b), respectively. Section Π obtain x, y values every periodic of rectangular wave force. The number of times the two torus touches the left boundary is denoted as L. In addition, the number of times it touches the upper boundary is denoted as U. In Fig. 5 (a.1), $L = 1$ and $U = 0$, and in Fig. 5 (a.3), $L = 2$ and $U = 1$. Between the parameter values at which Fig. 5 (a.1) and Fig. 5 (a.3) are obtained on the two-parameter Lyapunov diagram, the two-dimensional torus attractor with $L = 1 + 2 = 3$ and $U = 0 + 1 = 1$ exists as shown in Fig. 5 (a.2). Fig. 5(b.1), (b.2), and (b.3) show the associated experimental results. Remarkable agreement can be confirmed, and Farey sequence is observed.

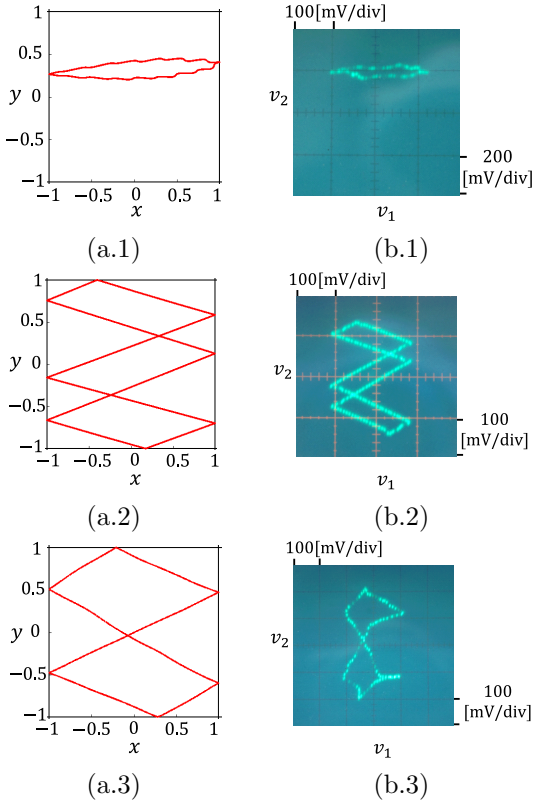

Figure 5: Numerical and associated experimental observation of Farey sequence. (a.1) $D_2 = 0.61$, $2T = 2.376$; (a.2) $D_2 = 0.68$, $2T = 2.376$; (a.3) $D_2 = 0.7168$, $2T = 2.4596$. (b.1) $V_{th2} = 655.7[mV]$, $2T_0 = 0.207[ms]$; (b.2) $V_{th2} = 597[mV]$, $2T_0 = 0.207$; and (b.3) $V_{th2} = 560[mV]$, $2T_0 = 0.214[ms]$

5. Conclusion

We discussed Chaos and bifurcation phenomena in a driven piecewise-constant oscillator. We used a calculation algorithm for the rigorous solutions in non-autonomous piecewise-constant system to conduct Lyapunov analysis. The explicit representation of the procedure can be applicable to a wide class of piecewise-constant driven circuit. Chaos is observed in the neighborhood of Chenciner bubbles. Moreover, the Farey sequence is observed in the experimental measurements. In future work, we plan to discuss quasiperiodic bifurcation in higher dimensional piecewise-constant oscillator.

References

[1] M. Sekikawa, N. Inaba, K. Kamiyama, and K. Aihara, "Three-dimensional tori and Arnold tongues," *Chaos*, vol.24, 013137, 2014.

[2] Y. P. Emelianova, A. P. Kuznetsov, L. V. Turukina, I. R. Sataev, N. Y. Chernyshov, "A structure of the oscillation frequencies parameter space for the system of dissipatively coupled oscillators," *Commun. Nonlinear Sci. Numer. Simulat.*, vol.19, pp. 1203-1212, 2014.

[3] T. Tsubone, N. Inaba, T. Tsubouchi, T. Yoshinaga, "Synchronization phenomena from an extremely simplified piecewise-constant driven oscillator," *IEICE Trans*, vol.J93-A, pp.375-383, 2010

[4] N. Inaba, K. Kamiyama, T. Kousaka, T. Endo, "Numerical and experimental observation of Arnold resonance webs in an electrical circuit," *Physica D*, 311-312, pp.17-24, 2015.

[5] K. Suzuki, T. Tsubone, "In-Phase and Anti-Phase synchronization phenomena in coupled systems of piecewise constant oscillators," *IEICE Trans. Fundamentals*, vol.E98-A, pp.340-353, 2015.

[6] C. Baesens, J. Guckenheimer, S. Kim, and R.S. Mackay, "Three coupled oscillators: mode-locking, global bifurcations and toroidal chaos," *Physica D*, vol.49, pp.387-475, 1991.